E3S Web of Conferences **730**, 02005 (2026) https://doi.org/10.1051/e3sconf/202673002005
Soft Soils 2026

Evolution of pore structure and creep characteristics of Indian black cotton soil under oedometer conditions

Venkata Balaiah Kami [1], and *Anumita* Mishra [1*]

[1] Department of Civil Engineering, Indian Institute of Technology Roorkee, Roorkee, Uttarakhand, India

Abstract. The present study investigated the macro- and micro-structural creep behavior of remolded Indian black cotton soil under various loading-unloading-reloading cycles. The macrostructural creep behavior of soil was evaluated using multi-stage oedometer tests (*MSL* tests) under two loading conditions with varying durations. The microstructural analysis included mineral identification using X-ray diffraction (*XRD*) and evaluation of pore morphology and particle rearrangements using scanning electron microscopy. The *XRD* analysis revealed a higher proportion of illite, which significantly affected inter-aggregate pores, resulting in a more pronounced reduction in pore area. The reduction in pore area was about 1.54-1.89 times at an intermediate stage of the *MSL* test and 2.48-3.74 times at the end of the *MSL* test. Although pore count reduction was 22-73% higher in the vertical plane (i.e., parallel to loading), pore area reduction was 26-64% higher in the transverse plane (i.e., perpendicular to loading). The predominance of micropores was greater in the vertical plane, resulting in a greater reduction in pore count. In contrast, the transverse plane has a significant number of small pores, whose reduction contributes more to the overall reduction in pore area. Rose diagrams revealed that the majority of pores were aligned between 150° and 225° at an early stage of consolidation, then reoriented to 150° and 195° at the intermediate stage, and finally uniformly distributed across all quadrants at the end of the test. The particle orientation index data also showed that the majority of pores initially exhibited anisotropic behavior and transitioned to isotropic behavior by the end of the *MSL* tests.

1 Introduction

Soft clayey soils, such as Indian black cotton soils, cover approximately one-fifth of the country's area and are abundant in the central and southern regions. Engineering structures, such as embankments, marine structures, earth-retaining structures, building foundations, highway and railway pavements, airport runways, and bridge abutments and piers, constructed on these soils exhibit gradual deformation over time due to their high compressibility and low shear strength. In addition, these soils undergo significant creep during loading and exhibit swelling upon unloading. Rapid industrial growth and urban development in India have led to the widespread use of soft soils as foundation materials for land reclamation and other infrastructure developments. The significant volume changes caused by swelling and creep can lead to excessive settlement, potentially damaging structures built on it. Therefore, it is essential to evaluate and predict the time-dependent stress-strain response of soft clays, which requires incorporating these time-dependent deformations into the design of structures on them. However, the macro-level response of these soils depends on microstructural changes within the soil matrix, including mineral composition, pore morphology, and particle arrangement. In addition, the changes in these soils are influenced by elastic deformation, dissipation of excess pore water pressure during consolidation, and viscous adjustments within the soil structure at constant effective stress (i.e., creep). Therefore, it is advisable to investigate both macro- and micro-structural behavior of soft clays under various loading, unloading, and reloading conditions.

Numerous studies have employed 1D oedometer tests and triaxial tests to investigate the macrostructural response of soft soils, such as Indian black cotton soils and Hong Kong marine deposits, under sustained loads and varying loading-unloading-reloading cycles [1-5]. These investigations have primarily focused on compressibility characteristics, including compression and rebounding indices, duration of primary consolidation, and secondary consolidation coefficient. However, understanding the microstructural behavior (i.e., particle and pore connections, particle sliding, compression of inter-aggregate pores, and structural adjustments within the soil matrix) under the same loading scenarios has remained limited [6-11]. The time-dependent response of soft clays, i.e., both creep and swelling, is primarily due to internal structural adjustments, delayed water transfer, compression of inter-aggregate pores, stress history, particle sliding, and viscous adjustment within the soil matrix [12-21]. Evaluating these processes at the macro level is difficult; therefore, it is essential to examine the stress-strain response at the microscopic level. To accomplish this,

* Corresponding author: mishra.anumita@gmail.com

several researchers have employed X-ray diffraction [6, 9] and scanning electron microscope [22-28] to investigate the mineralogical composition, creep characteristics and evolution of soil fabric.

The existing literature indicates that many studies have focused on the macroscopic evolution of creep during *MSL* tests and creep tests. However, investigations of the corresponding microstructural behavior of soft soils remain limited. Since the creep response of soil is influenced by its stress magnitude and duration, studies examining their effects on microstructural evolution are scarce. Furthermore, most researchers [23-25, 28] have focused primarily on general pore-related characteristics, including pore classification, identification of inter- and intra-aggregate pores, as well as their orientations. However, detailed assessments of how pore and particle morphology change under varying stress cycles and durations, including alterations in pore number, pore size and area, and particle orientation during 1D compression, have received limited attention [6, 29-32]. Kami and Mishra [31] investigated the microstructural evolution associated with creep during loading-unloading-reloading cycles in the vertical plane, which aligns with the direction of the applied load. A few studies have examined pore characteristics in the plane perpendicular to loading [6, 32]; however, investigations on particle morphology changes in this plane remain insufficient. Overall, previous studies have elucidated the general mechanisms of creep at the microstructural level, but a clear correlation between macroscopic and microscopic observations remains lacking. In this context, the present work focuses on the microstructural changes that occurred within the soil matrix during *MSL* load tests. The analysis considers different parameters, including load durations (i.e., before the test (t_0), intermediate stage (t_{60}), and end of *MSL* test (t_{120})), different loading patterns (i.e., *LP1* and *LP2* patterns), and different planes of observation (i.e., vertical plane and transverse plane). To achieve this, *MSL* tests were conducted first, followed by the extraction of specimens from the oedometer rings for *SEM* analysis. The *SEM* images were analyzed to evaluate changes in pore structure and particle arrangement within the soil matrix. In addition, *XRD* analysis was performed to identify the clay and non-clay minerals present in the soil sample. The interpretation of macro- and micro-structural test data to evaluate the evolution of creep of soft soils has been given attention in the present study.

2 Materials and methodology

2.1 Materials

The black cotton soil sample used here was transported from Sagar, Madhya Pradesh, India. Geotechnical characterization of the soil was determined following the Indian Standard and ASTM soil testing codes. Laboratory tests revealed a specific gravity of 2.65, an optimum moisture content of 22.7%, a maximum dry density of 16 kN/m^3, a liquid limit of 58.6%, and a plasticity index of 32.6%. Grain size analysis showed that the soil consisted of 58% silt, 39% clay, and 3% sand, classifying it as a highly compressible clay (CH).

2.2 Methodology

2.2.1 Macrostructural tests

1D multi-stage oedometer (*MSL*) tests were performed to evaluate the macrostructural response of soft soil under varying loading-unloading-reloading cycles. The consolidation behaviour of the soil is significantly affected by its initial moisture content and unit weight. The soil was initially prepared in a Proctor mould at its optimum moisture content and maximum dry density [3], then transferred into an oedometer ring. After achieving saturation, *MSL* tests were conducted to examine the time-dependent response. The loading sequence followed a predefined pattern in which the applied stress was approximately doubled at each stage, while during unloading, it was reduced to nearly half the previous value.

For the present analysis, two loading patterns were considered, as illustrated in Table 1.

1. LP1 pattern investigates the influence of stress cycles on the time-dependent behavior. In this case, the applied load lasted for 1 to 7 days, where the maximum load value, i.e., 1000 kPa, during loading and reloading cycles lasted for 7 days to examine creep behavior, and the minimum load value, i.e., 100 kPa, during unloading, lasted for 7 days to examine swelling behavior; all other intermediate loads were applied for 1 day.
2. LP2 pattern examines the influence of stress duration on the creep behavior, where each loading, unloading, and reloading stage was maintained for a duration of 7 days.

2.2.2 Microstructural tests

To examine the microstructural aspects of creep in soft clays, *XRD* analysis for identifying minerals and *SEM* tests for pore and particle characterization were conducted. Mineral identification was performed using a Bruker D8 Powder *XRD* instrument. For this analysis, fine powder with a particle size of less than 75 μm was used. In *XRD* patterns, quartz typically shows high-intensity peaks, whereas clay minerals show low-intensity peaks, making them difficult to identify. To address this, the centrifugation technique was adopted to separate finer clay fractions from silt particles, enabling clear detention of clay minerals. In this method, 0.25g of sodium hexametaphosphate was mixed with the soil as a dispersing agent, similar to that of the procedure followed in hydrometer laboratory tests. According to IS: 2720 (Part 4) – 1985, a minimum duration of 10-15 minutes is required for effective dispersion; thus, a dispersion time of 15 minutes was adopted in this study.

The *SEM* analysis has four phases: (1) sample collection from the consolidation ring, (2) obtaining *SEM* images, (3) image processing, and (4) observations and quantification. After *MSL* tests, *SEM* specimens measuring 10 mm in diameter and 20 mm in height were extracted from the consolidation ring at different load durations (t_0, t_{60}, and t_{120}) for both loading patterns (*LP1* and *LP2*). Before conducting *SEM* tests, a vacuum must be established within the *SEM* chamber. Due to the soil's porous nature, achieving the required vacuum is challenging; therefore, the sample height was trimmed to 10 mm to ensure proper vacuum conditions. The *SEM* images were taken using an Apreo Field Emission SEM with Low Vacuum.

Table 1. Test details for *MSL* tests.

Loading pattern	Cycle	Load value (kPa)	Duration (days)
LP1	loading	50	1
		100	1
		250	1
		500	1
		1000	7
	unloading	500	1
		250	1
		100	7
	reloading	250	1
		500	1
		1000	7
LP2	loading	50	7
		100	7
		250	7
		500	7
		1000	7
	unloading	500	7
		250	7
		100	7
	reloading	250	7
		500	7
		1000	7

*Note: The details of loading, first unloading, and reloading cycles have been provided in the above table.

The *SEM* images were analyzed using ImageJ, and an automated method was used to examine the time-dependent microstructural behavior of the soil. In this method, the raw *SEM* images were first converted to binary images, and pore and particle identification were performed using a suitable threshold in ImageJ. The *SEM* analysis was characterized into two: (1) general characterization, including pore classification, count, area, shape parameters (shape ratio, circularity and roundness), particle arrangement, as well as pore-particle interconnections before the *MSL* tests. (2) Time-dependent observations evaluated the changes in pore type, reduction in pore count and area, and particle rearrangements within the soil structure at t_{60} and t_{120}.

3 Results and discussion

3.1 Multi-stage oedometer test results

The variation in vertical strain over different time periods during stress cycles is illustrated in Figs. 1 and 2. For both the *LP1* and *LP2* patterns, the vertical strain-time (log scale) response remained almost constant at lower stress levels of 50 kPa and 100 kPa. In contrast, at higher stresses, i.e., 250 kPa, 500 kPa, and 1000 kPa, the curves showed a linear trend that progressively decreased until the end of primary consolidation (*EOP*), followed by a nominal variation over time. Meanwhile, during unloading, it initially exhibits a linear trend that gradually increases until *EOP*, and finally, minimal variation over time was observed for both loading patterns. However, the reloading cycle follows a consistent trend with that of the loading cycle. The time required to reach *EOP* (t_{EOP}) was estimated using Taylor's square root method for both loading patterns. By considering both loading patterns, t_{EOP} during the loading stage ranged from 14 to 109 minutes. However, for the unloading and reloading stages, these values were about 20 to 79 minutes and 18 to 80 minutes, respectively. Based on these results, the considered soil sample falls into the highly compressible clay category, consistent with the classification from the plasticity chart.

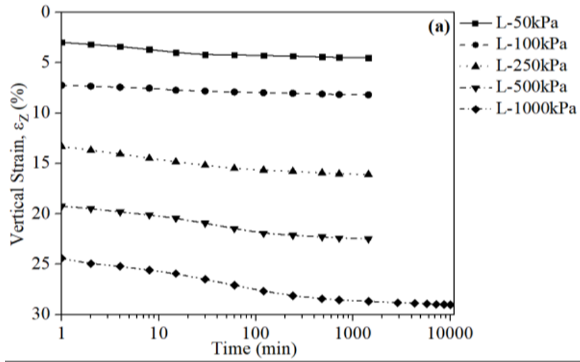

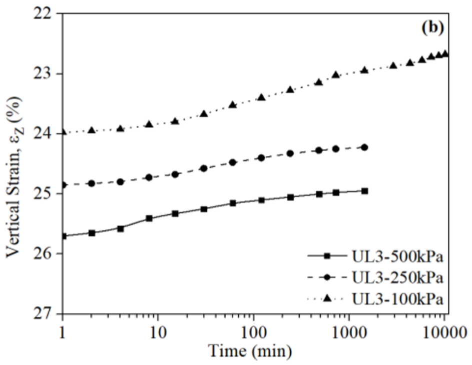

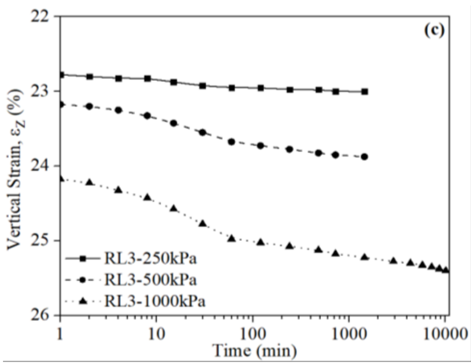

Fig. 1. Vertical strain versus time (log scale) curves for (a) loading cycle, (b) unloading cycle, and (c) reloading cycle under *LP1* pattern.

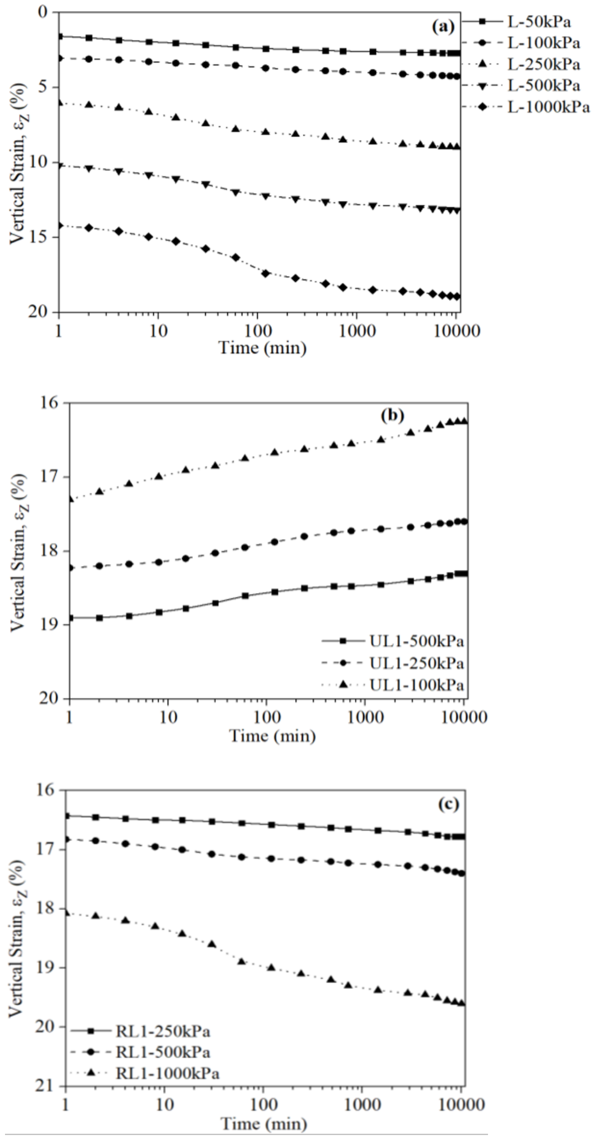

Fig. 2. Vertical strain versus time (log scale) curves for (a) loading cycle, (b) unloading cycle, and (c) reloading cycle under *LP2* pattern.

The compression and recompression parameters and indices were obtained from the vertical strain-vertical stress relationships and are summarized in Table 2. Each loading, unloading, and reloading response was processed using curve-fitting techniques in Origin 8.5.1 software [33], and the best fit was used to determine the compression parameter (λ/V) and the rebounding parameter (κ/V), as illustrated in Fig. 3. The term "V" denotes the specific volume and is equal to $1+e_o$. Where e_o represents the initial void ratio, which was calculated from the *MSL* tests and is equal to 0.55. The vertical strain versus vertical stress curves indicated a preconsolidation pressure of 100 kPa, resulting in an almost constant vertical strain over time. Table 2 indicates that the compression index (C_c/V) ranged from 0.08 to 0.11, whereas the rebounding index (C_r/V) ranged from 0.017 to 0.024. These trends closely mirror those of λ/V and κ/V, which were directly proportional to each other. Based on these observations, the material parameters of λ/V exhibited significant variation for both *LP1* and *LP2* patterns. This variation can be attributed to the influence of loading duration and stress history on the dissipation of excess pore water pressure and structural changes in the soil matrix, thereby altering the relationship between void ratio and effective stress. As a result, the calculated λ/V values vary with changes in the compressibility characteristics.

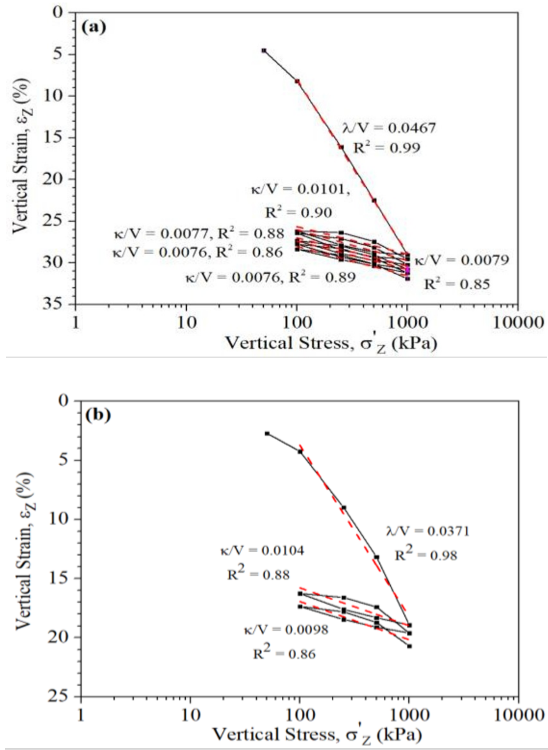

Fig. 3. Vertical strain versus vertical stress curves for (a) *LP1* pattern and (b) *LP2* pattern.

Table 2. Compression parameter and index, and rebounding parameter and index under both *LP1* and *LP2* patterns.

Loading pattern	Load cycle	λ/V	κ/V	C_c/V	C_r/V
LP1	L1	0.0467	-	0.1074	-
	RL1	-	0.0101	-	0.0232
	RL2	-	0.0079	-	0.0182
	RL3	-	0.0077	-	0.0177
	RL4	-	0.0076	-	0.0175
	RL5	-	0.0076	-	0.0175
LP2	L1	0.0371	-	0.0853	-
	RL1	-	0.0104	-	0.0239
	RL2	-	0.0098	-	0.0225

It was also inferred from the table that κ/V showed a slight reduction during the first stress cycle for both *LP1* and *LP2*, and remained unchanged for the remaining cycles in the *LP1* pattern. These observations indicate that the material properties of λ/V are influenced by loading characteristics, specifically the loading path and duration, while those of κ/V depend on both load magnitude and duration. It was also found that the secondary consolidation coefficient ($C_{\alpha e}/V$) ranged from 0.00137 to 0.00129 for the *LP1* and *LP2*, respectively. This coefficient is defined as the slope of the vertical strain-time curve after the completion of primary consolidation. Using the relationship between the creep coefficient (ψ^c/V) and secondary consolidation coefficient (i.e., ψ^c/V = ln(10) $C_{\alpha e}/V$), the creep coefficient values for *LP1* and *LP2* patterns were estimated at about 0.00315 and 0.00297, respectively. From these outcomes, it was observed that both $C_{\alpha e}/V$ and ψ^c/V for the *LP1* pattern were somewhat higher compared to those of the *LP2* pattern. This difference can be attributed to the sufficient time allowed for soil layer compression during the previous loads in the *LP2* pattern, which consequently led to a lower observed creep coefficient.

3.2 Microstructural analysis

The existence of clay minerals, pore structure and particle morphology significantly influenced their macro- and microstructural behaviour. Therefore, both mineral identifications based on *XRD* data and changes in pore structure and particle morphology, as observed in scanning electron microscope (*SEM*) images at various load values and durations, were discussed in this section. The *XRD* data indicated that clay minerals were predominantly identified at a lower Bragg's angle, i.e., between 5° and 36°. Table 3 illustrates the details of both clay and non-clay minerals present in the considered soil sample. The *XRD* data revealed that illite-group minerals were more pronounced than montmorillonite and interstratified illite-montmorillonite.

Table 3. X-ray diffraction data.

Mineral	Bragg's angle
Illite (I)	8.82°, 19.72° and 36°
Montmorillonite (M)	5.35°, 7.01° and 19.99°
Interstratified illite-montmorillonite (I-M)	6° to 20°

The pore structure and particle rearrangements were analyzed using the obtained *SEM* images. Consequently, the changes in pore structure (i.e., count, area, circularity, roundness, shape ratio, orientation) and particle orientation index under various parameters, such as load duration, loading pattern and observation planes, are discussed. Fig. 4 illustrates the existence of various pores under different load durations during the *MSL* tests. Based on the classification provided by Lei [34], the pores were termed as micropores (r_e < 1 μm), small pores (r_e: 1-4 μm), mesopores (r_e: 4-16 μm) and macropores (r_e > 16 μm) (where r_e represents equivalent pore radius).

From Fig. 4a, it was observed that micropores contributed predominantly to the total pore count during the initial loading stages. Once loading began, the larger pores were initially affected, and as consolidation progressed, the smaller pores tended to compress. At the initial loading stage (t_0), the pore count was high because no stress was applied. At t_{60}, there was a notable decrease of approximately 20-41% in the number of pores compared to t_0. This decline is primarily due to pore-water expulsion, resulting in the compression of the soil layer. Additionally, by the end of the *MSL* test (t_{120}), the pore count decreased by about 58-91% relative to t_0 and by about 50-77% compared to t_{60}. This decrease can be attributed to the sliding of particles and the subsequent structural rearrangements within the soil matrix, as illustrated in Fig. 5. Furthermore, the total reduction in pore area at t_{60} and t_{120} was approximately 1.54 to 1.89 times and 2.48 to 3.74 times lower than that observed in the initial stage, respectively.

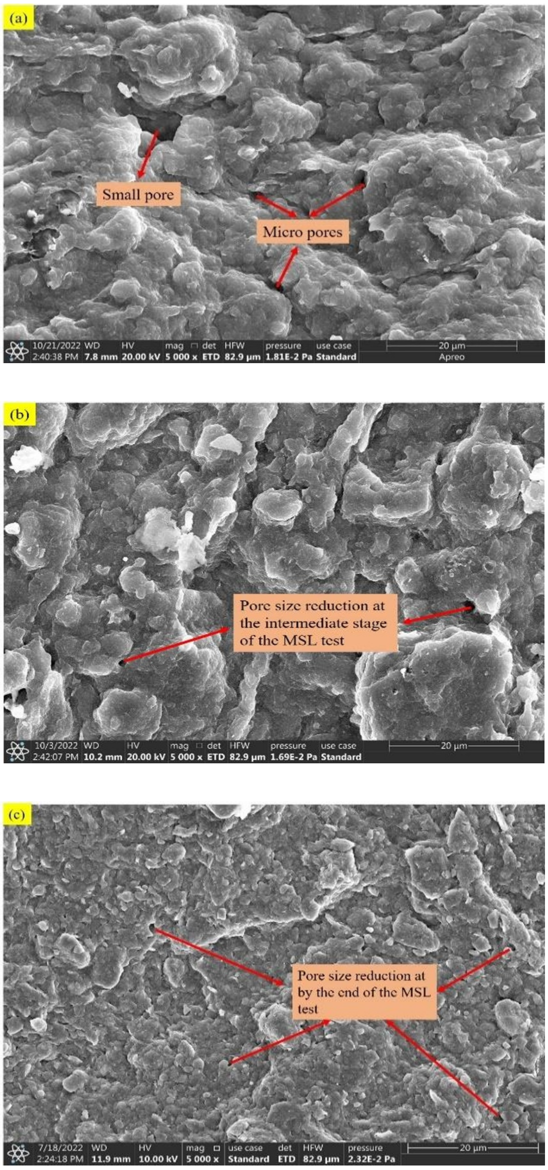

Fig. 4. Existence of pores at (a) t_0, (b) t_{60}, and (c) t_{120}.

It was also inferred that the reduction in pore count and pore area under the *LP2* pattern increased by about 16-25% and 4-16%, respectively, compared to the *LP1* pattern. This is because the soil sample under the LP2 pattern is subjected to a constant vertical stress for a specific period (i.e., 7 days), allowing the soil to undergo greater compression during the MSL tests and promoting greater compression of more inter-aggregate pores. Fig. 6 illustrates the changes in pore number and pore area under both vertical and transverse planes. It was observed that micropores were predominantly present in the vertical section across all soil samples, leading to a higher pore count compared to the transverse section. Specifically, pore number in the vertical section was about 1.22 to 1.73 times higher than that observed in the transverse section. As a result, the reduction in pore area was about 1.26-1.64 times greater in the transverse section than in the vertical section. This reduction is attributed to the fact that small pores were more pronounced in the transverse section; thus, their reduction contributed to a greater overall reduction in pore area.

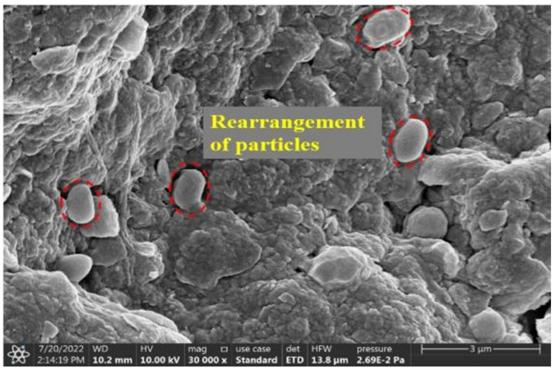

Fig. 5. Particles sliding and rearrangements within the soil matrix.

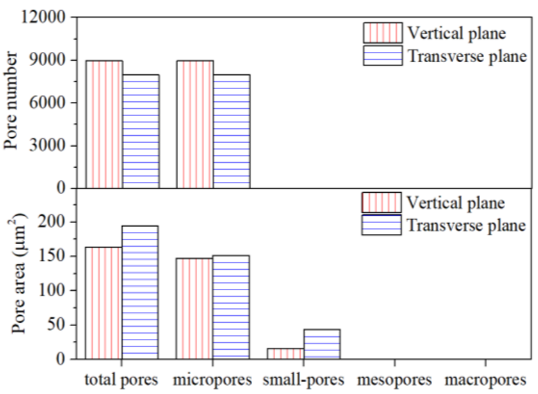

Fig. 6. Histograms of pore number and pore area for different planes of observation.

The results indicate that pore circularity and roundness showed minimal variation across different loading patterns and durations, and observation planes; hence, these aspects were not discussed in this work. Rose diagrams were employed to illustrate the orientation of pores and particles, with pore orientations evaluated relative to the horizontal axis of the fitted ellipse. For rose diagrams, 4-20 data points were considered per sample. As noted by Barton [35], approximately 400-500 measurements are generally required to obtain a statistically representative sample of both pore and particle orientation distributions. The observations showed that the pore alignment initially ranged from 150° to 225° at t0, then reoriented to 150°-195° at t_{60}, and finally uniformly aligned in all directions. Meanwhile, most pores were predominantly aligned between 195° and 240° for the *LP1* pattern and between 150° and 225° for the *LP2* pattern.

Fig. 7 illustrates the variation in pore orientations for both vertical and transverse sections. It was inferred from the figure that the large number of pores were aligned between 165°-240° in the vertical section and between 120°-195° in the transverse section. Particle orientations were determined from the angles of fitted ellipses, while the anisotropy was quantified using the orientation index. Prior to consolidation, most particles were aligned between 255° and 285°. At the intermediate stage, they ranged between 240° and 285°, and by the end of the test, they further reoriented to 255°-360°. The particle orientation index differentiates anisotropic (I_{or} = 0) from isotropic (I_{or} = 1) arrangements. Fig. 8 illustrates the changes in particle orientation index at different load durations for the *LP1* pattern. It was inferred that the particle arrangement was anisotropic before the test commenced. However, as consolidation progressed, the particles transitioned towards isotropic behaviour. The orientation index was estimated to be 0.51 at t_0, 0.70 at $t_{60,}$ and 0.76 at t_{120}.

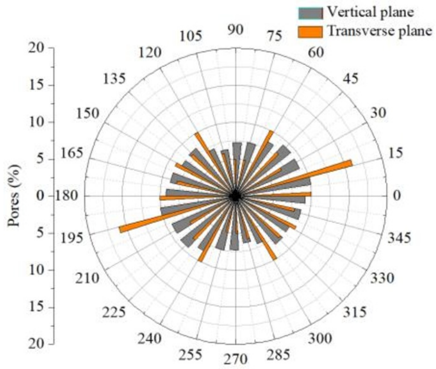

Fig. 7. Pore orientations for different planes of observation.

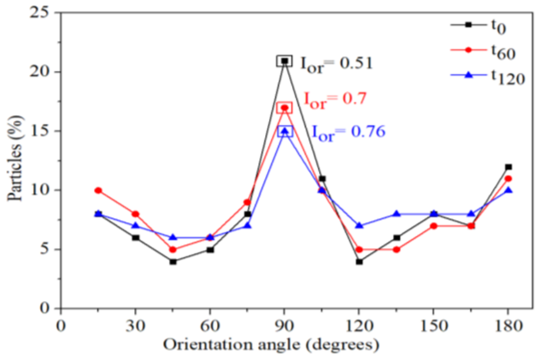

Fig. 8. Particle orientation index for different load durations.

Fig. 9 shows that loading patterns significantly affected particle orientations, as the percentage of particles varied across quadrants under both *LP1* and *LP2*. The orientation indices for the *LP1* and *LP2* patterns were estimated to be 0.79 and 0.99, respectively. It was also observed that the particle arrangement was more isotropic under *LP2* than under *LP1*. The variation in particle orientations and the particle orientation index for both vertical and transverse planes is illustrated in Fig. 10. It was observed that particle orientations varied across all quadrants in both sections. The orientation indices were about 0.81 and 0.73 for both vertical and transverse sections. Additionally, the estimated orientation index was higher in the transverse section than in the vertical section, indicating that particle arrangement in the transverse direction was more anisotropic.

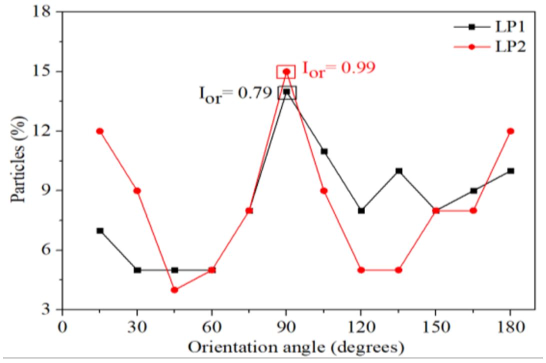

Fig. 9. Particle orientation index for different loading patterns.

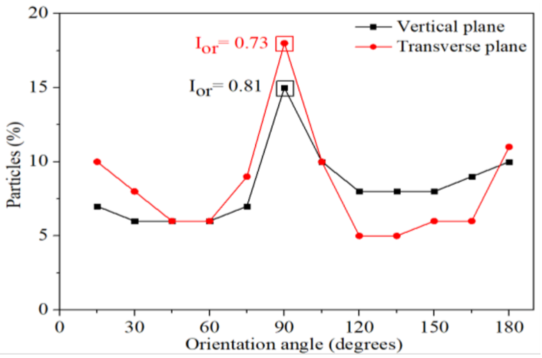

Fig. 10. Particle orientation index for different planes of observation.

3.3 Interpretation of macro- and micro-structural test results

The *MSL* tests revealed that the considered soil sample exhibited significant creep under both loading patterns. However, the unloading data showed nominal variation in swelling parameter and index up to two reloading cycles in the *LP1* pattern, indicating that the influence of subsequent stress cycles was almost negligible. Meanwhile, the *XRD* data revealed that the considered soil sample contained quartz, illite, montmorillonite, and interstratified illite-montmorillonite minerals, with illite being the predominant clay mineral. In general, the presence of illite minerals significantly influences soil swelling behavior due to their non-expansive nature; thus, a similar behavior was observed during reloading cycles in *MSL* tests. Quartz particles exhibited random orientations within the soil matrix, resulting in isotropic behaviour. Illite particles are predominantly oriented between 0-15°, especially 10°-15° [36], indicating that soils with high illite content have pronounced anisotropic behaviour. Montmorillonite particles are oriented between 0°-20°, while the orientation of interstratified illite-montmorillonite depends on the relative proportions of its components [37-38]. It was observed that the particle arrangement was anisotropic before the commencement of the tests; however, as consolidation progressed, it transitioned towards isotropic behaviour.

4 Conclusions

The key findings of this study are summarized below:

1. Under the *LP1* pattern, both the secondary consolidation coefficient and the creep coefficient decreased with increasing vertical stress. In contrast, these parameters remained nearly constant under the *LP2* pattern. This difference can be explained by the longer duration of load application in *LP2*, which provided the soil layer with ample time to compress during the initial loading stages, ultimately leading to reduced creep deformation.
2. The soil sample analyzed in this study primarily contained illite group minerals, which demonstrated a more uniform and repeatable rebound response throughout the *MSL* tests.
3. Micropores accounted for the majority of the total pore number, whereas small pores were small in number due to compression during *MSL* tests; however, they remained significant in pore area estimation.
4. The influence of load duration, loading patterns and plane of observations on pore circularity, aspect ratio and roundness was insignificant, while its influence on pore and particle orientations was more pronounced.
5. The particle orientation index confirmed that the particles exhibited isotropic behavior by the end of the *MSL* test in the vertical plane under the *LP2* pattern.

References

1. Q. Luo, X. Chen, Experimental research on creep characteristics of Nansha soft soil. Sci. World. J. 1, 968738 (2014).
https://doi.org/10.1155/2014/968738
2. W.Q. Feng, B. Lalit, Z.Y. Yin, J.H. Yin, Long-term nonlinear creep and swelling behavior of Hong Kong Marine deposits in oedometer condition. Comput. Geotech. **84**, 1-15 (2017).
3. M.J. Singh, F. Weiqiang, X. Dong-Sheng, L. Borana, Experimental study of compression behavior of Indian black cotton soil in oedometer condition. Int. J. Geosynth. Gr. Eng. **6**, 1–13 (2020).
4. X.B. Xu, Z.D. Cui, Investigation of a fractional derivative creep model of clay and its numerical implementation. Comput. Geotech. **119**,103387 (2020).
https://doi.org/ 10. 1016/j.compg eo.2019.103387
5. B.S. Olek, An experimental investigation of the influence of plasticity on creep degradation rate. Acta. Geotech. **17**, 803–817 (2022).
https:// doi. org/ 10. 1007/ s11440- 021- 01272-z
6. X. Xie, S. Qi, F. Zhao, D. Wang, Creep behavior and the microstructural evolution of loess-like soil from Xi'an area, China. Eng. Geol. **236**, 43–59 (2018).
https://doi. org/10.1016/j.enggeo.2017.11.003

7. P. Li, W. Xie, R.Y.S. Pak, Microstructural evolution of loess soils from the Loess Plateau of China. CATENA. **173**, 276–288 (2019).
https://doi.org/10.1016/j. catena.2018.10.006
8. I.A. Okewale, Compressibility and the effects of structure of Tropical Clay in Incremental Loading Oedometer tests. Geotech. Geol. Eng. **38**, 5355–5371 (2020). https://doi.org/10.1007/s10706-020-01369-4
9. Y.N. Wei, W. Fan, B. Yu, L.S. Deng, T. Wei, Characterization and evolution of three-dimensional microstructure of Malan loess. CATENA. **192** (2020). https://doi.org/10.1016/j.catena.2020.104585
10. Y. Wang, H. Yang, X. Jing, Structural characteristics of natural loess in Northwest China and its effect on shear behavior. Geotech. Geol. Eng. **39**, 65–78 (2021). https://doi.org/10.1007/s10706-020-01420-4
11. D. Zhao, M. Hattab, P.Y. Hicher, Z.Y. Yin, Effect of stress level on the microstructural evolution of clay under creep. J. Eng. Mech. **148**, 1–17 (2022).
12. B.G. Mesri, Coefficient of secondary compression. J. soil. Mech. Found. Div. **99**, 123–137 (1973).
13. P. Delage, G. Lefebvre, Study of the structure of a sensitive Champlain clay and of its evolution during consolidation. Can. Geotech. J. **21**, 21–35 (1984). https://doi.org/10.1139/ t84-003
14. L. Bjerrum, Engineering geology of Norwegian normally-consolidated marine clays as related to settlements of buildings. Geotechnique. **17**, 83–118 (1967). https://doi.org/10.1680/geot.1967.17.2.83

V. Navarro, E.E. Alonso, Secondary compression of clays as a local dehydration process. Geotechnique. **51**, 859–869 (2001). https://doi.org/10.1680/geot.2001.51.10.859
15. J.K. Mitchell, K. Soga, Fundamentals of soil behavior (Vol. 3, p. USA). New York: John Wiley and Sons (2005).
16. J.H. Yin, Calculation of settlements of foundation soils considering creep. In: Soft ground engineering in coastal areas. Proceedings of the Nakase memorial symposium 205 – 11 (2003).
17. T.M. Le, B. Fatahi, H. Khabbaz, Viscous behaviour of soft clay and inducing factors. Geotech. Geol. Eng. **30**, 1069 – 1083 (2012).
https://doi.org/10.1007/s10706- 012-9535-0
18. T. Ma, C. Wei, C. Yao, P. Yi, Microstructural evolu tion of expansive clay during drying–wetting cycle. Acta. Geotech. **15**, 2355–2366 (2020).
https://doi.org/10. 1007/s11440-020-00938-4
19. Q.F. Gao, L. Zeng, Z.N. Shi, R. Zhang, Evolution of unsaturated shear strength and microstructure of a compacted silty clay on wetting paths. Int. J. Geomech. **21**, 1–12 (2021).
20. B. Lian, X. Wang, H. Zhan, J. Wang, J. Peng, T. Gu, R. Zhu, Creep mechanical and microstructural insights into the failure mechanism of loess landslides induced by dry-wet cycles in the Heifangtai platform, China. Eng. Geol. **300**, 106589 (2022).
https://doi.org/10.1016/j. enggeo.2022.106589
21. P.Y. Hicher, H. Wahyudi, D. Tessier, Microstructural analysis of inherent and induced anisotropy in clay. Mech. Cohesive-Frictional. Mater. **5**, 341–371 (2000).
22. X. Zhang, L. Kong, A. Guo, Y. Tuo, Evolution of micro scopic pore of structured clay in compression process based on SEM and MIP test. Yanshilixue Yu Gongcheng Xuebao/Chinese. J. Rock. Mech. Eng. **31**, 406–412 (2012).
23. M. Hattab, T. Hammad, J.M. Fleureau, Internal friction angle variation in a kaolin/montmorillonite clay mix and microstructural identification. Geotechnique. **65**, 1–11 (2015). https://doi.org/10.1680/geot.13.P.081
24. H. Lei, H. Lu, X. Wang, Q. Ren, B. Li, Changes in soil micro-structure for natural soft clay under accelerated creep condition. Mar. Georesources. Geotechnol. **34**, 365 375 (2016).
https://doi.org/10.1080/10641.19X. 2015.10106 69
25. F. Cotecchia, S. Guglielmi, F. Cafaro, A. Gens, Characterization of the multi-scale fabric features of high plasticity clays. Geotech. Lett. **9**, 361–368 (2019). https://doi.org/10.1680/jgele.18.00230
26. J. Li, Y. Tang, W. Feng, Creep behavior of soft clay subjected to artificial freeze–thaw from multiple-scale perspectives. Acta. Geotech. **15**, 2849–2864 (2020). https://doi.org/10.1007/s11440-020-00980-2
27. J. Yuan, Y. Gan, J. Chen, S. Tan, J. Zhao, Experimental research on consolidation creep characteristics and microstructure evolution of soft soil. Front. Mater. **10**, 1–8 (2023).
https://doi.org/10.3389/fmats.2023.11373-24
28. R. Jia, H. Lei, K. Li, Compressibility and microstructure evolution of different reconstituted clays during 1D compression. Int. J. Geomech, **20**, 1-14 (2020).
29. D. Zhao, Q.F. Gao, M. Hattab, P.Y. Hicher, Z.Y. Yin, Microstructural evolution of remolded clay related to creep. Transp. Geotech, **24**, 100367 (2020). https://doi.org/10.1016/j.trgeo.2020.100367
30. V.B. Kami, A. Mishra, Microstructural analysis of creep in soft clays under loading and unloading stress cycles. Geotech. Geol. Eng, **42**, 1-19 (2024).
https://doi.org/10.1007/s10706-024-02941-y
31. V.B. Kami, A. Mishra, A comprehensive study on microstructural behavior of clay under oedometer condition. Bull. Eng. Geol. Environ, **84**, 107 (2025). https://doi.org/10.1007/s10064-025-04129-x
32. Origin 8.5.1 version, Northampton, MA: OriginLab Corporation (2011). https://www.originlab.com
33. X.Y. Lei, Pore types of loess soils in China and its collapsibility. Sci. China. B, **12**, 1310-1316 (1987).
34. C.M. Barton, The micromorphological soil-investigation work of Dr. D. Lafeber. In Soil Microscopy Proceedings of the International Working Meeting on Soil Micromorphology (1974).
35. H. Kodama, R.E. Grim, Clay mineral. Encyclopedia Britannica (2018).
36. R.H. Meade, Removal of water and rearrangement of particles during the compaction of clayey sediments. US Government Printing Office (1964).
37. M. Okawara, Y. Saito, K. Soga, Study on the mechanism of consistency characteristics of Na-montmorillonite using the small-angle X-ray scattering method. Clay Science, **23**, 9-24 (2019).